Self-diffusion and interdiffusion in $Al_{80}Ni_{20}$ melts: Simulation and experiment

J. Horbach,[1,2] S. K. Das,[1,3] A. Griesche,[4] M.-P. Macht,[4] G. Frohberg,[5] and A. Meyer[2]
[1]*Institut für Physik, Johannes-Gutenberg-Universität Mainz, Staudinger Weg 7, 55099 Mainz, Germany*
[2]*Institut für Materialphysik im Weltraum, Deutsches Zentrum für Luft- und Raumfahrt, 51170 Köln, Germany*
[3]*Institute for Physical Science and Technology, University of Maryland, College Park, Maryland 20742, USA*
[4]*Hahn-Meitner-Institut Berlin, Department Materials (SF3), Glienicker Strasse 100, 14109 Berlin, Germany*
[5]*Institut für Werkstoffwissenschaften und -technologien, Technische Universität Berlin, Hardenbergstrasse 36, 10623 Berlin, Germany*
(Received 9 February 2007; published 22 May 2007)

A combination of experimental techniques and molecular-dynamics computer simulation is used to investigate the diffusion dynamics in $Al_{80}Ni_{20}$ melts. Experimentally, the self-diffusion coefficient of Ni is measured by the long-capillary (LC) method and by quasielastic neutron scattering. The LC method yields also the interdiffusion coefficient. Whereas the experiments were done in the normal liquid state, the simulations provided the determination of both self-diffusion and interdiffusion constants in the undercooled regime as well. The simulation results show good agreement with the experimental data. In the temperature range $3000\ \mathrm{K} \geqslant T \geqslant 715\ \mathrm{K}$, the interdiffusion coefficient is larger than the self-diffusion constants. Furthermore, the simulation shows that this difference becomes larger in the undercooled regime. This result can be referred to a relatively strong temperature dependence of the thermodynamic factor Φ, which describes the thermodynamic driving force for interdiffusion. The simulations also indicate that the Darken equation is a good approximation, even in the undercooled regime. This implies that dynamic cross correlations play a minor role for the temperature range under consideration.

DOI: 10.1103/PhysRevB.75.174304 PACS number(s): 66.10.Cb, 64.70.Pf, 61.20.Ja

I. INTRODUCTION

Multicomponent liquids exhibit transport processes due to concentration fluctuations among the different components. In the hydrodynamic limit, these processes are described by interdiffusion coefficients.[1–3] In the simplest case of a binary AB mixture, there is one interdiffusion coefficient D_{AB}. This quantity plays an important role in many phenomena seen in metallic mixtures, such as solidification processes,[4] the slowing down near the critical point of a liquid-liquid demixing transition,[5] and glassy dynamics.[6]

Many attempts have been undertaken for different binary systems to relate D_{AB} to the self-diffusion constants D_A and D_B via phenomenological formulas (see, e.g., Refs. 7–12). An example is the Darken equation[13] that is widely used to estimate the interdiffusion constant of simple binary fluid mixtures. This equation expresses D_{AB} as a simple linear combination of the self-diffusion coefficients, $D_{AB} = \Phi(c_B D_A + c_A D_B)$ (with c_A and c_B being the mole fractions of A and B particles, respectively). Here, the so-called thermodynamic factor Φ contains information about static concentration fluctuations in the limit of long wavelengths.

The relationship between one-particle transport and collective transport properties is a fundamental question in undercooled liquids.[6] In the framework of the mode-coupling theory of the glass transition, Fuchs and Latz[14] have studied a binary 50:50 mixture of soft spheres with a size ratio of 1.2. Their numerical data indicate that the Darken equation is a good approximation for the latter system in the undercooled regime. However, from experiments or computer simulations, not much is known about the validity of the Darken equation for undercooled liquids. This is due to the lack of experimental data for interdiffusion coefficients in this case. Moreover, most of the computer simulation studies on the relation between self-diffusion and interdiffusion have been only devoted to the normal liquid state. In this case, the Darken equation often seems to work quite well.[1,10,12,15,16]

In this work, a combination of experiment and molecular-dynamics (MD) simulation is used to study the diffusion dynamics in the metallic liquid $Al_{80}Ni_{20}$. In the MD simulation, the interactions between the atoms are modeled by an embedded atom potential proposed by Mishin *et al.*[17] The present work is a continuation of a recent study,[18] where a combination of quasielastic neutron-scattering (QNS) and MD simulation was applied to investigate chemical short-ranged order and self-diffusion in the Al-Ni system at different compositions. In the latter study, we have shown that the MD simulation yields good agreement with the QNS data, both for structural quantities and the Ni self-diffusion constant, D_{Ni}. In the present work, an additional experimental method, the long-capillary (LC) technique, is used. This method allows us to determine simultaneously the self-diffusion constant D_{Ni} and the interdiffusion coefficient D_{AB} (see below).

Above the liquidus temperature (i.e., in the normal liquid state), thermodynamic properties as well as structure and dynamics of $Al_{80}Ni_{20}$ have been studied by different approaches (see, e.g., Refs. 15 and 19–23). The Al-Ni system is an ordering system which is manifested in a negative enthalpy of mixing.[24] Thus, it does not exhibit a liquid-liquid miscibility gap where one would expect that the interdiffusion coefficient vanishes when approaching the critical point, whereas the self-diffusion constants are not affected by the critical slowing down (see Ref. 25 and references therein). Such a behavior is not expected for the Al-Ni system.

In the computer simulation, the $Al_{80}Ni_{20}$ melt can be undercooled to an arbitrary extent, avoiding the occurrence of crystallization processes. Therefore, we were able to study a broad temperature range in our MD simulations, ranging

from the normal liquid state at high temperature to the undercooled liquid at low temperature. In the experiments presented below, crystallization occurs due to heterogeneous nucleation. Thus, the experiments were performed above the liquidus temperature $T_L \approx 1280$ K. The combination of experiment and simulation presented in this work allows for a test of the validity of the Darken equation in $Al_{80}Ni_{20}$. We will see below that this equation is indeed a good approximation, even in the undercooled regime.

In the next section, we summarize the basic theory on self-diffusion and interdiffusion. The details of the experiments and simulation are given in Secs. III and IV, respectively. In Sec. V we present the results. Finally, we give a summary of the results in Sec. VI.

II. SELF-DIFFUSION AND INTERDIFFUSION: BASIC THEORY

Consider a three-dimensional, binary AB system of $N=N_A+N_B$ particles (with N_A and N_B being the number of A and B particles, respectively). The self-diffusion constant $D_{s,\alpha}$ (α=A,B) is related to the random-walk motion of a tagged particle of species α on hydrodynamic scales. It can be calculated from the velocity autocorrelation function,[1]

$$C_\alpha(t) = \frac{1}{3N_\alpha}\sum_{j=1}^{N_\alpha} \langle \mathbf{v}_j^{(\alpha)}(t)\cdot \mathbf{v}_j^{(\alpha)}(0)\rangle, \tag{1}$$

via a Green-Kubo integral,

$$D_{s,\alpha} = \int_0^\infty C_\alpha(t)dt. \tag{2}$$

In Eq. (1), $\mathbf{v}_j^{(\alpha)}(t)$ is the velocity of particle j of species α at time t.

The self-diffusion constant can be also expressed by long-time limit of the mean-squared displacement (MSD),

$$D_{s,\alpha} = \lim_{t\to\infty} \frac{1}{N_\alpha}\sum_{j=1}^{N_\alpha} \frac{\langle [\mathbf{r}_j^{(\alpha)}(t) - \mathbf{r}_j^{(\alpha)}(0)]^2\rangle}{6t}. \tag{3}$$

Here, $\mathbf{r}_j^{(\alpha)}(t)$ is the position of particle j of species α at time t. Note that Eq. (3) is equivalent to the Green-Kubo formula (2).

Interdiffusion is related to the collective transport of mass driven by concentration gradients. The transport coefficient that describes this process is the interdiffusion constant D_{AB} which can be also expressed by a Green-Kubo relation, i.e., by a time integral over an autocorrelation function. The relevant variable in this case is the concentration or interdiffusion current[1] given by

$$\mathbf{J}_{AB}(t) = \sum_{i=1}^{N_A} \mathbf{v}_i^{(A)}(t) - c_A\left[\sum_{i=1}^{N_A} \mathbf{v}_i^{(A)}(t) + \sum_{i=1}^{N_B} \mathbf{v}_i^{(B)}(t)\right], \tag{4}$$

where $c_A \equiv N_A/N = 1-c_B$ is the total concentration (mole fraction) of A particles. As a matter of fact, the autocorrelation function of the variable $\mathbf{J}_{AB}(t)$ depends on the reference frame, and fluctuations of $\mathbf{J}_{AB}(t)$ have to be adapted to the ensemble under consideration. Whereas experiments are usually done in the canonical ensemble, in a molecular-dynamics simulation, the natural ensemble is the microcanonical ensemble with zero total momentum.[26] Thus,

$$\sum_{i=1}^{N_B} \mathbf{v}_i^{(B)} = -\frac{m_A}{m_B}\sum_{i=1}^{N_A} \mathbf{v}_i^{(A)} \tag{5}$$

follows, where m_A and m_B denote the masses of A and B particles, respectively. Introducing the "center-of-mass velocity of component α (α=A,B)" by

$$\mathbf{V}_\alpha(t) = \frac{1}{N_\alpha}\sum_{i=1}^{N_\alpha} \mathbf{v}_i^{(\alpha)}(t), \tag{6}$$

we can use expression (5) to simplify the formula for the interdiffusion current,

$$\mathbf{J}_{AB}(t) = Nc_Bc_A\left(1 + \frac{m_Ac_A}{m_Bc_B}\right)\mathbf{V}_A(t). \tag{7}$$

Thus, we have to consider only the velocities of one species to compute $\mathbf{J}_{AB}(t)$.

Now, the autocorrelation function for the interdiffusion current is given by

$$\begin{aligned} C_{AB}(t) &= \langle \mathbf{J}_{AB}(t)\cdot \mathbf{J}_{AB}(0)\rangle \\ &= N^2(c_Bc_A)^2\left(1 + \frac{m_Ac_A}{m_Bc_B}\right)^2 \langle \mathbf{V}_A(t)\cdot \mathbf{V}_A(0)\rangle. \end{aligned} \tag{8}$$

The Green-Kubo formula for D_{AB} reads

$$D_{AB} = \frac{1}{3NS_{cc}(0)}\int_0^\infty C_{AB}(t)dt, \tag{9}$$

where $S_{cc}(0)$ is the concentration-concentration structure factor in the limit $q\to 0$. The function $S_{cc}(q)$ is the static correlation function associated with concentration fluctuations. It can be expressed by a linear combination of partial static structure factors $S_{\alpha\beta}(q)$ (α,β=A,B) as follows:[1]

$$S_{cc}(q) = c_B^2S_{AA}(q) + c_A^2S_{BB}(q) - 2c_Ac_BS_{AB}(q), \tag{10}$$

with

$$S_{\alpha\beta}(q) = \frac{1}{N}\sum_{k=1}^{N_\alpha}\sum_{l=1}^{N_\beta} \langle \exp[i\mathbf{q}\cdot(\mathbf{r}_k - \mathbf{r}_l)]\rangle. \tag{11}$$

Using the elementary fluctuation theory,[1] $S_{cc}(0)$ can be related to the second derivative of the molar Gibbs free energy g,

$$\Phi = \frac{c_Ac_B}{k_BT}\frac{\partial^2 g}{\partial c_A \partial c_B}, \tag{12}$$

via

$$\Phi = \frac{c_Ac_B}{S_{cc}(q=0)}. \tag{13}$$

In Eq. (12), k_B is the Boltzmann constant and T the temperature. In the following, we will refer to Φ as the thermodynamic factor.

We note that the total structure factor for the number density, $S_{nn}(q)$, and the cross correlation between number density and concentration, $S_{nc}(q)$, can also be written as linear combinations of partial structure factors. These functions are given by[1]

$$S_{nn}(q) = S_{AA}(q) + 2S_{AB}(q) + S_{BB}(q), \tag{14}$$

$$S_{nc}(q) = c_B S_{AA}(q) - c_A S_{BB}(q) + (c_B - c_A) S_{AB}(q). \tag{15}$$

The typical behavior of these functions for a liquid mixture will be discussed in Sec. V. The functions $S_{nn}(q)$, $S_{nc}(q)$, and $S_{cc}(q)$ are often called Bhatia-Thornton structure factors.[27] In principle, these functions can be determined in neutron-scattering experiments, either by using isotopic enrichment techniques (see, e.g., Ref. 21) or by applying a combination of neutron scattering and x-ray diffraction.[28]

With Eqs. (9) and (13), the interdiffusion constant can be written as

$$D_{AB} = N\frac{c_A c_B \Phi}{3}\left(1 + \frac{m_A c_A}{m_B c_B}\right)^2 \int_0^\infty \langle \mathbf{V}_A(t) \cdot \mathbf{V}_A(0)\rangle dt. \tag{16}$$

Alternatively, D_{AB} can be also easily related to the self-diffusion constants to yield

$$D_{AB} = \Phi[c_A D_B + c_B D_A + c_A c_B \int_0^\infty (\Lambda_{AA} + \Lambda_{BB} - 2\Lambda_{AB}) dt], \tag{17}$$

where the functions $\Lambda_{\alpha\beta}(t)$ denote distinct velocity correlation functions,

$$\Lambda_{\alpha\beta}(t) = \frac{1}{3Nc_\alpha c_\beta} \sum_{k=1}^{N_\alpha} \sum_{\substack{l=1 \\ l\neq k \text{ if } \alpha=\beta}}^{N_\beta} \langle \mathbf{v}_k^{(\alpha)}(t) \cdot \mathbf{v}_l^{(\beta)}(0)\rangle. \tag{18}$$

Note that the three functions $\Lambda_{\alpha\beta}(t)$ can be expressed by the "center-of-mass" correlation function $C_{AB}(t)$ and the velocity autocorrelation functions $C_\alpha(t)$ [the latter, multiplied by $1/c_\alpha$, has to be subtracted in the case of $\Lambda_{AA}(t)$ and $\Lambda_{BB}(t)$].[11] Thus, the functions $\Lambda_{\alpha\beta}(t)$ do not contain any additional information compared to $C_{AB}(t)$ and $C_\alpha(t)$, and so we do not consider them separately in the following.

If one denotes the distinct part in Eq. (17) by

$$\Delta_d = c_A c_B \int_0^\infty [\Lambda_{AA}(t) + \Lambda_{BB}(t) - 2\Lambda_{AB}(t)] dt, \tag{19}$$

one can rewrite Eq. (17) as

$$D_{AB} = \Phi S(c_A D_B + c_B D_A), \tag{20}$$

with

$$S = 1 + \frac{\Delta_d}{c_A D_B + c_B D_A}. \tag{21}$$

The quantity S measures the contribution of cross correlations to D_{AB}. If $S=1$ holds, the interdiffusion constant is determined by a linear combination of the self-diffusion constants. In this case, Eq. (20) leads to the Darken equation.[13] Note that in the context of chemical diffusion in crystals, S is called the Manning factor.[29]

As in the case of self-diffusion, the interdiffusion constant can be also expressed via a mean-squared displacement which involves now the center-of-mass coordinate of species A,

$$\mathbf{R}_A(t) = \frac{1}{N_A} \sum_{j=1}^{N_A} \mathbf{r}_j^{(A)}(t). \tag{22}$$

Then, the "Einstein relation" for D_{AB} reads

$$D_{AB} = \lim_{t\to\infty} \left(1 + \frac{m_A c_A}{m_B c_B}\right)^2 N c_A c_B \Phi \frac{\langle [\mathbf{R}_A(t) - \mathbf{R}_A(0)]^2 \rangle}{6t}. \tag{23}$$

This formula can be used to determine D_{AB} in a computer simulation, where the system is located in a simulation box with periodic boundary conditions. However, in this case, one has to be careful because the difference $\mathbf{R}_A(t) - \mathbf{R}_A(0)$ has to be calculated in an origin independent representation.[30] This can be achieved by computing this difference via the integral $\int_0^t \mathbf{V}_A(t')dt'$.

III. EXPERIMENTAL METHODS

A. Long-capillary technique

The LC technique has been used to measure interdiffusion and Ni self-diffusion in liquid $Al_{80}Ni_{20}$. The sample material production is similar to that of $Al_{87}Ni_{10}Ce_3$, which is described in Ref. 31. The experimental apparatus, the measurement of the concentration profiles, and the evaluation of the concentration profiles, including the determination of Fick's diffusion coefficients, are also described elsewhere.[32,33] Thus, here, the experimental technique is reported only briefly. In more detail, we describe an improved diffusion couple setup, which has been used in this work. This setup, with a vertical diffusion capillary of 1.5 mm diameter, has an increased stabilization against natural convection and minimizes the systematic error of convective mass flow contributions to the total mass transport.

The improvement of the diffusion couple setup implies the combination of interdiffusion and self-diffusion measurements in one experiment. An $Al_{80}Ni_{20}$ slice of 2 mm thickness, containing the enriched stable ^{62}Ni isotope, is placed between both rods of an interdiffusion couple. The interdiffusion couple consists of a 15-mm-long rod of $Al_{85}Ni_{15}$, placed above the slice, and a 15-mm-long rod of $Al_{75}Ni_{25}$, placed below the slice. This configuration allows the development of an error function shaped chemical interdiffusion profile simultaneously with the development of a Gauss function shaped self-diffusion profile. In a first approximation, the diffusion of the enriched stable isotope takes place at the mean concentration of $Al_{80}Ni_{20}$ without the influence of the changing chemical composition of the melt in the diffusion zone. The only necessary correction results from the mass spectrometric measurement of the self-diffusion

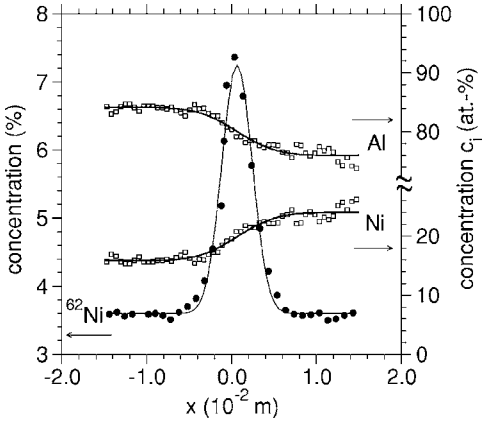

FIG. 1. Typical concentration profiles of combined interdiffusion and self-diffusion experiments. The squares denote the Al and Ni concentrations measured by energy-dispersive x-ray spectrometry, and the dots denote the ^{62}Ni concentration measured by inductively coupled plasma mass spectrometry. The lines represent the best fit (least-squares method) of the appropriate solution of Fick's diffusion equations to the measured concentrations.

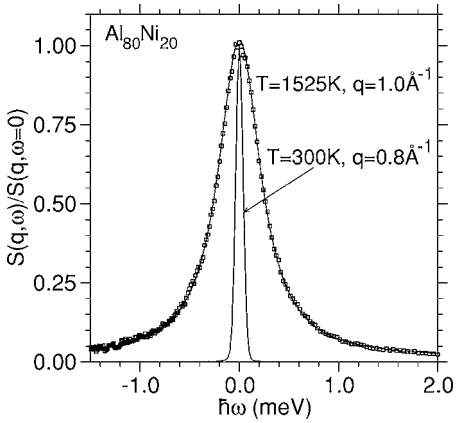

FIG. 2. Normalized scattering law of liquid $Al_{80}Ni_{20}$. The data at 300 K represent the instrumental energy resolution function. The line is a fit with a Lorentzian function that is convoluted with the instrumental energy resolution function. The diffusive motion of the atoms leads to a broadening of the quasielastic signal from which the Ni self-diffusivity can be obtained on an absolute scale.

profile. Here, the measured isotope incidences $i(^{62}\mathrm{Ni})$ of ^{62}Ni have to be corrected for the overlaying chemical concentration profile of natural Ni, c_{Ni}, by using the following formula:

$$c(^{62}\mathrm{Ni}) = c_{\mathrm{Ni}}[i(^{62}\mathrm{Ni}) - i(^{62}\mathrm{Ni}^0)], \tag{24}$$

with $i(^{62}\mathrm{Ni}^0)$ being the natural incidence of ^{62}Ni and $c(^{62}\mathrm{Ni})$ the concentration of this Ni isotope with respect to all Ni isotopes. Typical concentration profiles of a diffusion experiment are given in Fig. 1.

The diffusion couple configuration minimizes the risk of convection compared to conventional self-diffusion experiments in pure melts because of the solutal stabilized density profile of the melt column. This stabilizing effect has been described in Refs. 34 and 35. In a standard self-diffusion experiment without chemical gradient the solutal stabilization effect is only due to the enrichment of a tracer.

As a test for other mass transport processes we measured the mean-square penetration depth $\bar{x}^2$ of interdiffusion as a function of time t. We found a deviation from the linear behavior $\bar{x}^2 = 2D_{\mathrm{AB}}t$. This has been identified as sedimentation of Al_3Ni_2 during solidification of the diffusion sample. This additional mass transport was simply corrected by subtracting this contribution as an offset of the measured total mass transport. This procedure adds a 5%–10% error to the uncertainty of the diffusion coefficient. The total error in the long-capillary measurements of the self-diffusion and interdiffusion coefficients is about 30%–40%.

B. Neutron-scattering experiments

The second experimental technique used in this work is quasielastic neutron scattering. In this case, the $Al_{80}Ni_{20}$ alloy was prepared by arc melting of pure elements under a purified argon atmosphere. The measurements were done at the time-of-flight spectrometer IN6 of the Institut Laue-Langevin. The standard Nb resistor high-temperature vacuum furnace of the ILL exhibits a temperature gradient over the entire sample at 1800 K that was less than five degrees and a temperature stability within one degree. For the scattering experiment, we used a thin-walled Al_2O_3 container that provides a hollow cylindrical sample geometry of 22 mm in diameter and a sample wall thickness of 1.2 mm.

An incident neutron wavelength of $\lambda = 5.1$ Å yielded an energy resolution of $\delta E \simeq 92$ μeV (fill width at half maximum) and an accessible wave-number range at zero energy transfer of $q = 0.4$–2.0 Å^{-1}. Measurements were performed at 1350, 1525, 1670, and 1795 K in 2 h runs each. A run at room temperature provided the instrumental energy resolution function. The scattering law $S(q,\omega)$ was obtained by normalization to a vanadium standard, accompanied by a correction for self-absorption and container scattering, and interpolation to constant wave numbers q. Further, $S(q,\omega)$ was symmetrized with respect to the energy transfer $\hbar\omega$ by means of the detailed balance factor.

Figure 2 displays $S(q,\omega)$ at $q = 1.0$ Å^{-1} of liquid $Al_{80}Ni_{20}$ at 1525 K and the crystalline alloy at 300 K at $q = 0.8$ Å^{-1}. The diffusive motion in the liquid leads to a broadening of the quasielastic signal. The data were fitted with a Lorentzian function that is convoluted with the instrumental energy resolution function. From the full width at half maximum of the quasielastic line Γ a q-dependent diffusion coefficient $D(q)$ can be computed via $D(q) = \Gamma/(2\hbar q^2)$. Toward small q, incoherent scattering on the Ni atoms dominates the signal and the diffusion coefficient $D(q)$ becomes constant, yielding an estimate of $D_{s,\mathrm{Ni}}$. Thus, the self-diffusion constant $D_{s,\mathrm{Ni}}$ can be determined on an absolute scale.[36,37]

IV. DETAILS OF THE SIMULATION

For the computer simulations of the binary system $Al_{80}Ni_{20}$, we used a potential of the embedded atom type that was recently derived by Mishin *et al.*[17] In a recent publication,[18] we have shown that this potential reproduces

very well structural properties and the self-diffusion constant of Al-Ni melts at various compositions. The present simulations are performed in a similar way as the ones in the latter work: Systems of $N=1500$ particles ($N_{Ni}=300$ and $N_{Al}=1200$) are put in a cubic simulation box with periodic boundary conditions. First, standard Monte Carlo simulations in the NpT ensemble[38] were used to fully equilibrate the systems at zero pressure and to generate independent configurations for MD simulations in the microcanonical ensemble. In the latter case, Newton's equations of motion were integrated with the velocity Verlet algorithm using a time step of 1.0 fs at temperatures $T \geqslant 1500$ K and 2.5 fs at lower temperatures.

The masses were set to 26.981 539 and 58.69 amu for aluminum and nickel, respectively. At each investigated temperature, we made sure that the duration of the equilibration runs exceeded the typical relaxation times of the system. The temperatures considered were 4490, 2994, 2260, 1996, 1750, 1496, 1300, 1100, 998, 940, 893, 847, 810, 777, 754, 735, 715, 700, 680, and 665 K. In order to improve the statistics of the results, we averaged each temperature over eight independent runs. At the lowest temperature, the duration of the microcanonical production runs were 40×10^6 time steps, thus yielding a total simulation time of about 100 ns. The latter production runs were used to study the tagged particle dynamics. For the calculation of the interdiffusion constant D_{AB}, additional production runs were performed in the temperature range $4490\ \text{K} \geqslant T \geqslant 715$ K that extended the production runs for the tagged particle dynamics by about a factor of 10. This was necessary in order to obtain a reasonable statistics for D_{AB}. Note that D_{AB} is a collective quantity that does not exhibit the self-averaging properties of the self-diffusion constant, and thus it is quite demanding to determine transport coefficients such as the interdiffusion constant or the shear viscosity from a MD simulation.

V. RESULTS

In Eq. (20), the interdiffusion constant D_{AB} is expressed as a linear combination of the self-diffusion constants. The prefactor in this formula is a product of the thermodynamic factor Φ and the Manning factor S. Whereas Φ can be computed from the structural input, the Manning factor contains the collective dynamic correlations in the expression for D_{AB} (see Sec. II). In the following, we compare the simulated diffusion constants for $Al_{80}Ni_{20}$ to those from experiments. Moreover, the simulations are used to disentangle differences between self-diffusion constants and the interdiffusion constants with respect to the thermodynamic quantity Φ and the dynamic quantity S.

First, we discuss static structure factors at different temperatures, as obtained from the MD simulation. Figure 3 displays the different partial structure factors at the temperatures $T=2000$ K and $T=750$ K. At both temperatures, a broad prepeak around the wave number $q=1.8$ Å^{-1} emerges in the NiNi correlations, which indicates the presence of chemical short-ranged order (CSRO). This feature is absent in the AlAl correlations. In a recent work,[18] we have found that the prepeak in $S_{NiNi}(q)$ is present in a broad variety of

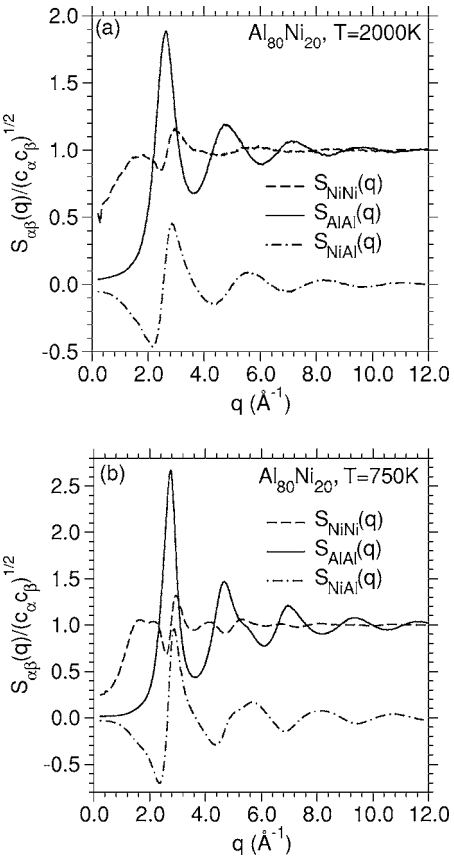

FIG. 3. Partial structure factors, as obtained from the MD simulation, at (a) $T=2000$ K and (b) $T=750$ K. The multiplication by $1/(c_\alpha c_\beta)^{1/2}$ is introduced to increase the amplitude of $S_{NiNi}(q)$ relative to that of $S_{AlAl}(q)$. Note that the factor $1/(c_\alpha c_\beta)^{1/2}$ leads also to the asymptotic value $S_{\alpha\alpha}(q)=1$ for $q \to \infty$.

Al-Ni compositions, ranging from $x_{Ni}=0.1$ to $x_{Ni}=0.9$. However, the width of the prepeak decreases significantly with increasing Ni concentration, and in melts with a high Ni concentration, it appears also in $S_{AlAl}(q)$. The prepeak in $S_{\alpha\beta}(q)$ describes repeating structural units involving next-nearest $\alpha\beta$ neighbors which are built in inhomogeneously into the structure. Of course, for the Al rich $Al_{80}Ni_{20}$ system considered in this work, only next-nearest Ni-Ni units exhibit the CSRO that is reflected in the prepeak.

From the partial static structure factors, the Bhatia-Thornton structure factors can be determined according to Eqs. (10), (14), and (15). These quantities are shown in Fig. 4, again at $T=2000$ K and at $T=750$ K. Although these structure factors look very different for $q>2$ Å^{-1}, they are essentially identical in the limit $q \to 0$. As we have indicated before, the static susceptibility, associated with concentration fluctuations, can be extracted from the structure factor $S_{cc}(q)$ in the limit $q \to 0$. As we can infer from Fig. 4, at the temperature $T=750$ K the value of this susceptibility is very small. The small value of $S_{cc}(q=0)$ reveals that concentration fluctuations on large length scales are strongly suppressed. This is the typical behavior of a dense fluid that exhibits a strong ordering tendency. In contrast, at a critical point of a demixing transition a divergence of $S_{cc}(q=0)$ is expected.

As we have seen in Sec. II, the ratio D_{AB}/Φ can be expressed as a linear combination of the self-diffusion con-

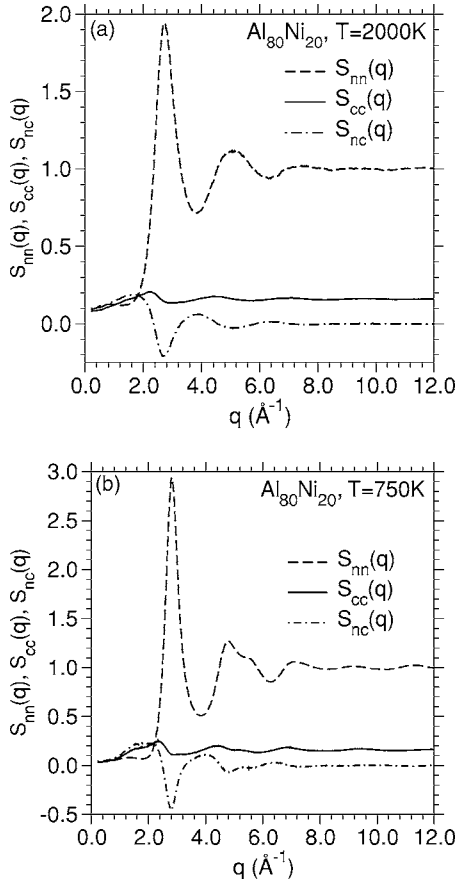

FIG. 4. Bhatia-Thornton structure factors, as obtained from the MD simulation, at (a) $T=2000$ K and (b) $T=750$ K.

stants, provided $S=1$ holds. In order to quantify the temperature dependence of S, we first define the following mean-squared displacements:

$$\langle r^2(t)\rangle_{\text{int}} = \left(1 + \frac{m_A c_A}{m_B c_B}\right)^2 N c_A c_B \langle [\mathbf{R}_A(t) - \mathbf{R}_A(0)]^2\rangle, \quad (25)$$

$$\langle r^2(t)\rangle_{\text{self}} = c_A \frac{1}{N_B}\sum_{j=1}^{N_B} \langle [\mathbf{r}_j^{(B)}(t) - \mathbf{r}_j^{(B)}(0)]^2\rangle + c_B \frac{1}{N_A}\sum_{j=1}^{N_A} \langle [\mathbf{r}_j^{(A)}(t) - \mathbf{r}_j^{(A)}(0)]^2\rangle. \quad (26)$$

Whereas the interdiffusion constant can be calculated via $D_{AB}=\lim_{t\to\infty}\Phi\langle r^2(t)\rangle_{\text{int}}/(6t)$, the equation $D_{AB}=\lim_{t\to\infty}\Phi\langle r^2(t)\rangle_{\text{self}}/(6t)$ is only correct for $S=1$. Figure 5 shows the quantities $\langle r^2(t)\rangle_{\text{int}}$ and $\langle r^2(t)\rangle_{\text{self}}$ for the different temperatures. Both MSD's show a very similar behavior. At high temperature, a crossover from a ballistic regime ($\propto t^2$) at short times to a diffusive regime ($\propto t$) at long times can be seen. At low temperature, a plateaulike region develops at intermediate times, i.e., between the ballistic and diffusive regimes. With decreasing temperature, the plateau becomes more pronounced. In $\langle r^2(t)\rangle_{\text{self}}$, the plateau indicates the so-called cage effect.[6] The tagged particle is trapped by its neighbors on a time scale that increases with decreasing temperature. Although the MSD for the interdiffusion, $\langle r^2(t)\rangle_{\text{int}}$, describes also the collective particle transport, the plateau in this quantity has the same origin: The particles are "arrested" on intermediate time scales. Moreover, the differences between $\langle r^2(t)\rangle_{\text{self}}$ and $\langle r^2(t)\rangle_{\text{int}}$ are anyway very small in the whole time and temperature range under consideration. This means that the cross correlations do not give a large contribution to $\langle r^2(t)\rangle_{\text{int}}$.

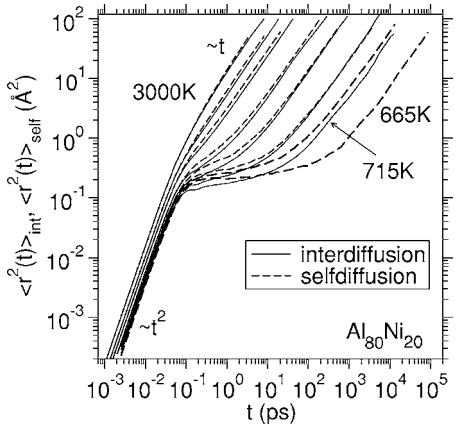

FIG. 5. Simulation results of mean-squared displacements (MSDs) for self-diffusion (dashed lines) and interdiffusion (solid lines) for the temperatures $T=3000$, 2000, 1500, 1000, 850, 750, 715, and 665 K (corresponding to the curves from left to right). Note that for $T=665$ K only $\langle r^2(t)\rangle_{\text{self}}$ was calculated. For the definitions of the MSD's, see Eqs. (25) and (26).

From the MSD's in Fig. 5, the Manning factor S can be extracted using Eq. (21). In Fig. 6 we see that the Manning factor varies only slightly over the whole temperature range, located around values between 0.8 and 1.0. Also shown in Fig. 6 is the thermodynamic factor Φ and the product ΦS. We have extracted Φ from the extrapolation of the structure factors $S_{cc}(q)$ toward $q\to 0$ [see Eq. (13)]. In contrast to the Manning factor S, the thermodynamic factor Φ increases significantly with decreasing temperature, and, thus, also the change in the product ΦS is dominated by the change in Φ. Therefore, differences in the qualitative behavior between the self-diffusion constants and the interdiffusion constant are dominated by the thermodynamic factor.

An Arrhenius plot of the diffusion constants as obtained from simulation and experiment is shown in Fig. 7. The self-

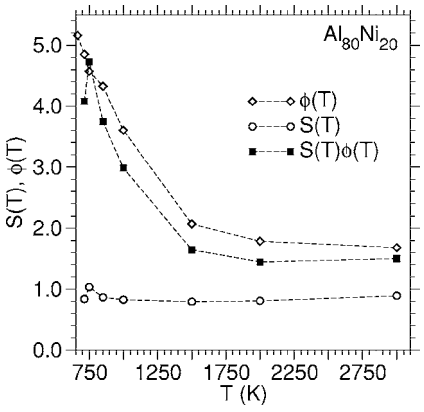

FIG. 6. Thermodynamic factor ϕ, "Manning" factor $S(T)$, and the product of both as obtained from the simulation.

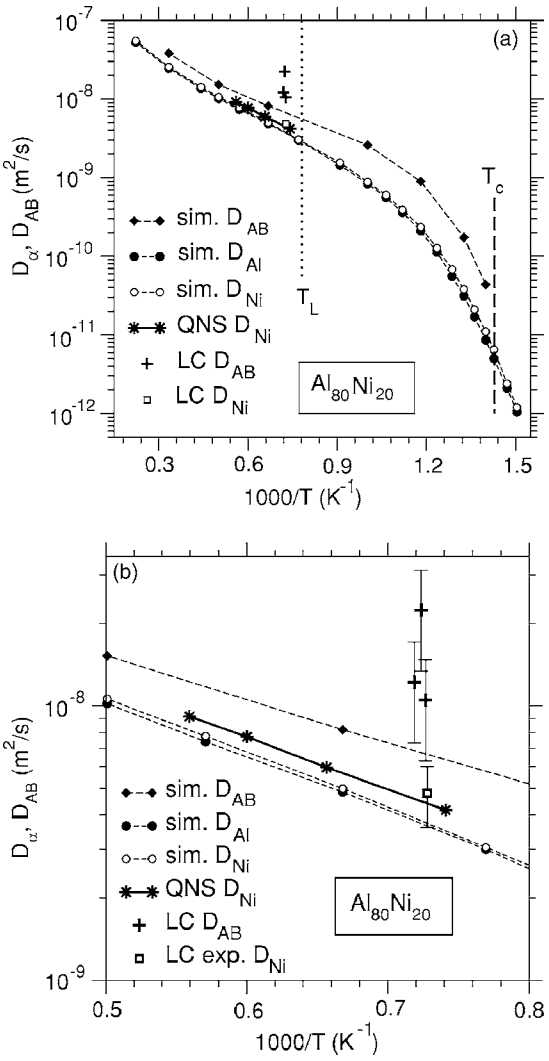

FIG. 7. Arrhenius plot of interdiffusion and self-diffusion constants, as obtained from experiment and simulation, as indicated. The experimental results are measured by quasielastic neutron scattering (QNS) and by the LC technique. The lines through the data points are guides to the eye. The vertical dotted line in (a) marks the location of the experimental liquidus temperature, $T_L \approx 1280$ K. The vertical dashed line is at the location of the critical temperature of the mode-coupling theory, $T_c \approx 700$ K, as estimated by the MD simulation (Ref. 41). Panel (b) is an enlargement of the data of panel (a) in a temperature range above T_L. The error bars of simulation and QNS data are of the order of the size of the symbols.

diffusion constants D_{Ni} and D_{Al} from the simulation are very similar over the whole temperature range of 4490 K $\geqslant T \geqslant$ 665 K. In a recent publication,[18] we have found that in the framework of our simulation model, this similarity of the self-diffusion constants occurs in Al rich compositions of the Al-Ni system, say, for $c_{Al} > 0.7$. Whether this is also true in real systems is an open question. However, the neutron-scattering results for D_{Ni} as well as the single point obtained from the LC measurement are in very good agreement with the simulation data.

Asta *et al.*[15] have computed the concentration dependence of the self-diffusion constants at $T=1900$ K using two different embedded atom potentials, namely, the one proposed by Voter and Chen[39] and the one proposed by Foiles and Daw.[40] For both potentials, they find very similar values for D_{Ni} and D_{Al} in $Al_{80}Ni_{20}$, in agreement with our results. However, their results for the Ni diffusion constant are significantly higher than the ones found in our quasielastic neutron-scattering experiment and our simulation. They report the values $D_{Ni} \approx 1.5 \times 10^{-8}$ m^2/s and $D_{Ni} \approx 1.9 \times 10^{-8}$ m^2/s for the Voter-Chen potential and the Foiles-Daw potential, respectively, whereas we obtain $D_{Ni} \approx 10^{-8}$ m^2/s from simulation and experiment. Thus, the potential proposed by Mishin *et al.*,[17] which is used in this work, leads to a better agreement with the experiment, as far as self-diffusion in $Al_{80}Ni_{20}$ is concerned.

We emphasize that the statistical error in both the neutron-scattering data and the simulation data for the self-diffusion constants is relatively small. In both cases, the error bars for the corresponding data points in Fig. 7 are smaller than the size of the symbols.

Due to the lack of self-averaging, it is much more difficult to yield accurate results for D_{AB} from the simulation. Therefore, in this case, we considered a smaller temperature range than for the self-diffusion constants to yield results with reasonable accuracy. As we can infer from Fig. 7, the interdiffusion constant is larger than the self-diffusion constants over the whole temperature range. The difference becomes more pronounced with decreasing temperature. At $T=715$ K, the diffusion coefficient D_{AB} is about a factor of 3 larger than D_{Ni} and D_{Al}. This behavior is, of course, due to the increase of the thermodynamic factor Φ at low temperature. Also included in Fig. 7 are the results of the LC measurements of D_{AB} and D_{Ni}. These results are much less accurate than those of the quasielastic neutron-scattering experiments for the determination of D_{Ni} [see the error bars for the LC data in Fig. 7(b)]. Nevertheless, the LC data show that $D_{AB} > D_{Ni}$ holds, in agreement with the simulation results.

VI. CONCLUSION

A combination of experiment and molecular-dynamics simulation has been used to investigate the diffusion dynamics in liquid $Al_{80}Ni_{20}$. We find good agreement between simulation and experiment. Both in experiment and in simulation, the interdiffusion constant is higher than the self-diffusion constants. This is valid in the whole temperature range considered in this work, i.e., in the normal liquid state as well as in the undercooled regime. In the latter regime (which is only accessible by the simulation), the difference between the interdiffusion constant and the self-diffusion constants increases with decreasing temperature.

All these observations can be clarified by the detailed information provided by the MD simulation. Both the thermodynamic factor Φ and the Manning factor S have been estimated directly and accurately over a wide temperature range, and so do self-diffusion and interdiffusion coefficients. The central result of this work is shown in Fig. 6. Whereas the thermodynamic factor Φ increases significantly by lowering the temperature, the Manning factor S shows only a weak temperature dependence. Moreover, the value of S is close to

1 which means that dynamic cross correlations are almost negligible, and, thus, even in the undercooled regime, the Darken equation is a good approximation. The temperature dependence of Φ is plausible for a dense binary mixture with a strong ordering tendency. The situation is similar to the case of the isothermal compressibility which normally decreases with temperature in a densely packed liquid, leading to very low values in the undercooled regime. In the same sense, the response to a macroscopic concentration fluctuation described by $S_{cc}(q=0)$ tends to become smaller and smaller towards the undercooled regime which corresponds to an increase of Φ with decreasing temperature [since $\Phi \propto 1/S_{cc}(q=0)$].

We note that the data shown for D_{AB} are all above the critical temperature T_c of mode-coupling theory which is around 700 K for our simulation model (see Fig. 7).[41] Since it is expected that the transport mechanism changes below T_c,[6] it would be interesting to see how such a change in the transport mechanism is reflected in the interdiffusion constants. This issue is the subject of forthcoming studies.

ACKNOWLEDGMENTS

We are grateful to Kurt Binder for stimulating discussions and a critical reading of the manuscript. We gratefully acknowledge the financial support within the SPP 1120 of the Deutsche Forschungsgemeinschaft (DFG) under Grants No. Bi314/18, No. Ma1832/3-2, and No. Me1958/2-3 and from DFG Grant No. Gr2714/2-1. One of the authors was supported through the Emmy Noether program of the DFG, Grant No. Ho2231/2-1/2 (J.H.). Computing time on the JUMP at the NIC Jülich is gratefully acknowledged.

[1] J.-P. Hansen and I. R. McDonald, *Theory of Simple Liquids* (Academic, London, 1986).
[2] M. Shimoji and T. Itami, *Atomic Transport in Liquid Metals* (Trans. Tech. Publications, Aedermannsdorf, 1986).
[3] A. R. Allnatt and A. B. Lidiard, Rep. Prog. Phys. **50**, 373 (1987).
[4] *Physical Metallurgy*, edited by R. W. Cahn and P. Haasen (North-Holland, Amsterdam, 1983), Pts. 1 and 2.
[5] P. C. Hohenberg and B. I. Halperin, Rev. Mod. Phys. **49**, 435 (1977).
[6] K. Binder and W. Kob, *Glassy Materials and Disordered Solids: An Introduction to Their Statistical Mechanics* (World Scientific, London, 2005).
[7] R. Vogelsang and C. Hoheisel, Phys. Rev. A **38**, 6296 (1988); H. P. van den Berg and C. Hoheisel, *ibid.* **42**, 2090 (1990).
[8] K. W. Kehr, K. Binder, and S. M. Reulein, Phys. Rev. B **39**, 4891 (1989).
[9] W. Hess, G. Nägele, and A. Z. Akcasu, J. Polym. Sci., Part B: Polym. Phys. **28**, 2233 (1990).
[10] J. Trullàs and J. A. Padró, Phys. Rev. E **50**, 1162 (1994).
[11] A. Baumketner and Ya. Chushak, J. Phys.: Condens. Matter **11**, 1397 (1999).
[12] J.-F. Wax and N. Jakse, Phys. Rev. B **75**, 024204 (2007).
[13] L. S. Darken, Trans. AIME **180**, 430 (1949).
[14] M. Fuchs and A. Latz, Physica A **201**, 1 (1993).
[15] M. Asta, D. Morgan, J. J. Hoyt, B. Sadigh, J. D. Althoff, D. de Fontaine, and S. M. Foiles, Phys. Rev. B **59**, 14271 (1999).
[16] F. Faupel, W. Frank, M.-P. Macht, H. Mehrer, V. Naundorf, K. Rätzke, H. R. Schober, S. K. Sharma, and H. Teichler, Rev. Mod. Phys. **75**, 237 (2003).
[17] Y. Mishin, M. J. Mehl, and D. A. Papaconstantopoulos, Phys. Rev. B **65**, 224114 (2002).
[18] S. K. Das, J. Horbach, M. M. Koza, S. Mavila Chatoth, and A. Meyer, Appl. Phys. Lett. **86**, 011918 (2005).
[19] G. L. Batalin, E. A. Beloborodova, and V. G. Kazimirov, *Thermodynamics and the Constitution of Liquid Al Based Alloys* (Metallurgy, Moscow, 1983).
[20] G. D. Ayushina, E. S. Levin, and P. V. Geld, Russ. J. Phys. Chem. **43**, 2756 (1969).
[21] M. Maret, T. Pomme, A. Pasturel, and P. Chieux, Phys. Rev. B **42**, 1598 (1990).
[22] S. Sadeddine, J. F. Wax, B. Grosdidier, J. G. Gasser, C. Regnaut, and J. M. Dubois, Phys. Chem. Liq. **28**, 221 (1994).
[23] M. Asta, V. Ozolins, J. J. Hoyt, and M. van Schilfgaarde, Phys. Rev. B **64**, 020201(R) (2001).
[24] V. S. Sudovtseva, A. V. Shuvalov, and N. O. Sharchina, Rasplavy **4**, 97 (1990); U. K. Stolz, I. Arpshoven, F. Sommer, and B. Predel, J. Phase Equilib. **14**, 473 (1993); K. V. Grigorovitch and A. S. Krylov, Thermochim. Acta **314**, 255 (1998).
[25] S. K. Das, J. Horbach, and K. Binder, J. Chem. Phys. **119**, 1547 (2003); S. K. Das, J. Horbach, K. Binder, M. E. Fisher, and J. V. Sengers, *ibid.* **125**, 024506 (2006); S. K. Das, M. E. Fisher, J. V. Sengers, J. Horbach, K. Binder, Phys. Rev. Lett. **97**, 025702 (2006).
[26] F. O. Raineri and H. L. Friedman, J. Chem. Phys. **91**, 5633 (1989); **91**, 5642 (1989).
[27] A. B. Bhatia and D. E. Thornton, Phys. Rev. B **2**, 3004 (1970).
[28] D. Holland-Moritz, O. Heinen, R. Bellissent, T. Schenk, and D. M. Herlach, Z. Metallkd. **97**, 948 (2006).
[29] J. R. Manning, Phys. Rev. **124**, 470 (1961).
[30] M. P. Allen, D. Brown, and A. J. Masters, Phys. Rev. E **49**, 2488 (1994); M. P. Allen, *ibid.* **50**, 3277 (1994).
[31] A. Griesche, F. Garcia-Moreno, M. P. Macht, and G. Frohberg, Mater. Sci. Forum **508**, 567 (2006).
[32] A. Griesche, M. P. Macht, J. P. Garandet, and G. Frohberg, J. Non-Cryst. Solids **336**, 173 (2004).
[33] A. Griesche, M. P. Macht, and G. Frohberg (unpublished).
[34] J. P. Garandet, C. Barrat, and T. Duffar, Int. J. Heat Mass Transfer **38**, 2169 (1995).
[35] C. Barrat and J. P. Garandet, Int. J. Heat Mass Transfer **39**, 2177 (1996).
[36] A. Meyer, Phys. Rev. B **66**, 134205 (2002).
[37] S. Mavila Chathoth, A. Meyer, M. M. Koza, and F. Yuranji, Appl. Phys. Lett. **85**, 4881 (2004).
[38] D. P. Landau and K. Binder, *A Guide to Monte Carlo Simulations in Statistical Physics* (Cambridge University Press, Cambridge, 2000).
[39] A. F. Voter and S. P. Chen, in *Characterization of Defects in Materials*, MRS Symposia Proceedings No. 82, edited by R. W. Siegel *et al.* (Materials Research Society, Pittsburgh, 1978), p. 175.
[40] S. M. Foiles and M. S. Daw, J. Mater. Res. **2**, 5 (1987).
[41] S. K. Das, J. Horbach, and K. Binder (unpublished).